Fracture mechanics of hybrid composites with ductile matrix and brittle fibers: Influence of temperature and constraint effect

B Vieille[1], J-D Gonzalez[1] and C Bouvet[2]

Abstract

The fracture behavior of hybrid carbon and glass fiber woven-ply reinforced polyether ether ketone thermoplastic quasi-isotropic laminates is investigated. Single-edge-notch bending and single-edge-notch tensile tests were conducted at room temperature and at a temperature higher than the glass transition temperature (T_g) to study the influence of both the constraint effect and the temperature on the strain energy release rate in laminates with ductile polyether ether ketone matrix and brittle fibers. As failure is primarily driven by fibers breakage in tension (single-edge-notch tensile test) and in tension/compression (single-edge-notch bending), it turns out that a temperature increase has very little influence on the mode I critical translaminar fracture toughness K_{Ic} though the ductility of polyether ether ketone matrix is exacerbated at $T > T_g$. It also appears that the constraint effect has very little influence on K_{Ic} as single-edge-notch tensile test and single-edge-notch bending specimens have virtually the same mean value (about 45MPa. $\sqrt{m}$). Single-edge-notch bending specimens being characterized by a gradual failure, the G-R curves were derived from the computation of the compliance loss and the corresponding gradual crack growth in agreement with the ASTM standard E1820. From the evolution of the G-R curves at high temperature, the highly ductile behavior of the polyether ether ketone matrix at $T > T_g$ provides a good intrinsic toughness to the material, and the bridging of translaminar crack by the glass fibers at the outer surfaces of laminates contribute to a moderate increase in its extrinsic toughness.

Keywords

Fracture mechanics, high temperature, mechanical testing, R-curves, thermoplastic

Introduction

In a material, fracture toughness is classically defined as the energy required to extend a crack, in other words to resist fracture under mechanical loading by means of locally dissipative behaviors (e.g. plastic deformation or damage mechanisms). In notched structures, plastic and damage deformation mechanisms are instrumental in redistributing the overstresses around the notch, and therefore in modifying their fracture behavior.[1 3] Early in the seventies, it was shown that the fracture toughness of engineering materials is improved by introducing tough fibers into a brittle matrix,[4] or brittle fibers into a ductile matrix.[5] In polymer matrix composites (PMCs), it is also well accepted that the insertion of a ductile resin-rich layer between laminates' layers is found to increase significantly their fracture resistance, without altering its dependence on crack growth rate.[6,7] The fiber/matrix adhesion also plays a major role in fracture toughness as the adhesion rules the overstress profiles in the vicinity of the fiber/matrix interface.[8] In brittle matrices polymer composites, a too strong interface discourages additional energy absorbing mechanisms such as fiber bridging and breakage.[3] In tough matrices polymer composites, the strong fiber/matrix interface is necessary to allow extensive deformation of the matrix in order to fully utilize the intrinsic matrix toughness.[9] The question is still open when it

[1]INSA Rouen, Groupe de Physique des Matériaux, France
[2]Institut Clément Ader, Université de Toulouse, France

Corresponding author:
B Vieille, INSA Rouen avenue de l'université St Etienne du Rouvray, 76801 France.
Email: benoit.vieille@insa-rouen.fr

comes to evaluate the influence of temperature and constraint effect on the translaminar fracture toughness of ductile thermoplastic (TP)-based composites with brittle fibers.[8,10,11] When a notched laminate is loaded in tension, a Fracture Process Zone (FPZ) is observed at the notch tip,[12] and gradually grows with increasing load (Figure 1). Depending on stacking sequence and constitutive materials, the crack path observed in fiber-reinforced polymer laminates is often complex. The crack propagates at a critical load, and the translaminar crack growth resulting from an initial transverse notch is usually self-similar (Figure 2) in quasi-isotropic brittle laminates.[13 16] Thus, the extension of a self-similar translaminar crack allows a global analysis based on a global strain energy-release rate that is computed from tensile loading.[14 17]

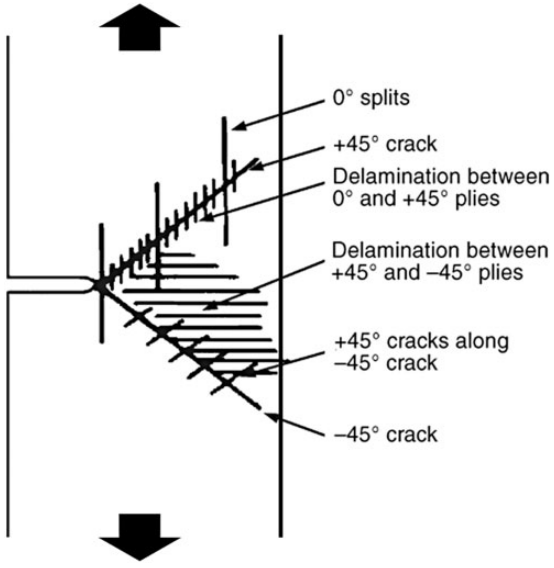

Figure 1. Typical fracture process zone at a sharp crack in single edge notch composites loaded in opening mode.[12]

In most engineering materials, the fracture resistance depends on their microstructure by means of two primary toughening (intrinsic and extrinsic) mechanisms.[1] As pointed by Launey et al.,[3] single-value parameters (such as the mode I critical stress intensity factor K_{Ic}) based on crack initiation are classically used to quantify intrinsic toughness (associated with the nature of the constituents and the reinforcement architecture). However, these parameters cannot always capture the ability of a microstructure to develop toughening mechanisms acting either ahead or behind the crack tip. The fracture toughness of fiber-reinforced composites is improved by increasing both micro- and meso-structural resistances by changing the nature of constituents, the fibers and matrix distribution and/or the interface properties to suppress damage (primarily micro-cracking and fiber breakage) ahead of the crack tip. These changes represent intrinsic toughening and are instrumental in increasing the fracture toughness of ductile materials. On the contrary, the fracture of brittle materials is characterized by micro- and meso-structural mechanisms. These mechanisms result in effectively reducing the crack-driving force at the crack tip by dissipating mechanical energy by means of local plastic deformation, damage mechanisms, and fibers bridging (primarily associated with local debonding and fibers pull-out). These mechanisms represent extrinsic toughening also known as crack-tip shielding.[3] Contrary to intrinsic toughness, extrinsic toughness is often developed primarily during crack growth resulting from crack-tip shielding mechanisms that result in rising R-curve behavior.

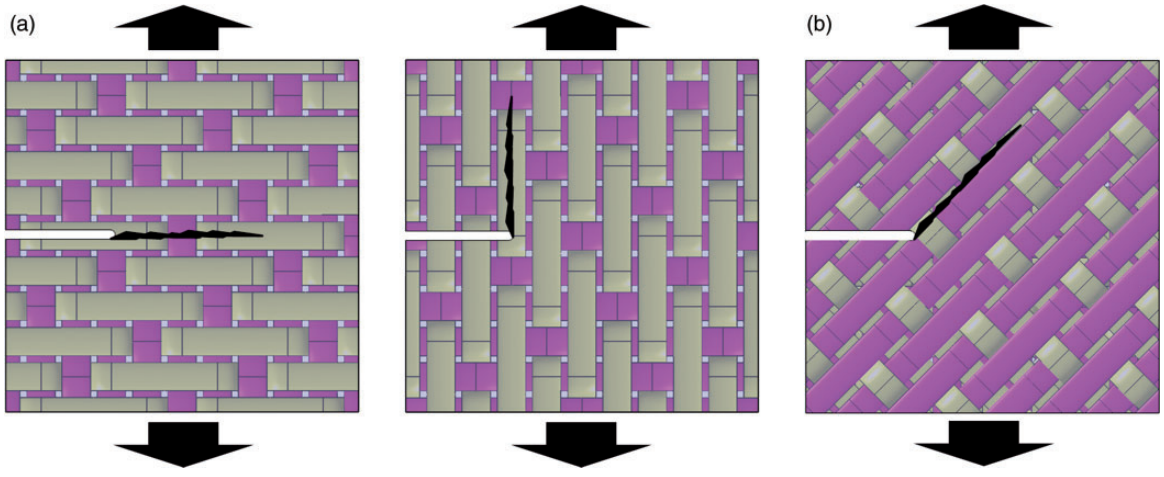

Figure 2. Crack growth in single edge notch laminates (Adapted from Jones[13]): (a) Self similar and (b) nonself similar.

The modes of energy dissipation are mainly affected by the matrix fracture mode (brittle or ductile). This is mainly determined by the loading rate or temperature conditions in the literature.[18 20]

The energy dissipated during controlled crack propagation in fiber-reinforced composites is usually evaluated in terms of different source mechanisms: plastic deformation, fiber-snapping, matrix-cracking, and fiber pull-out.[13,15,21] In composite materials with a brittle matrix, the energies dissipated during crack initiation and propagation in the composite with a weak fiber/matrix interface are derived principally from the work of fiber pull-out (resulting from the frictional forces that hold a broken fiber in its matrix socket). In ductile matrix composite systems, the local plastic deformation of the matrix must also be taken into account in the total fracture toughness.[19,22] The mechanical behavior of polymer resins exhibits temperature dependence (viscoelastic and viscoplastic behaviors) not only above glass transition temperature (T_g) but also below T_g. Kim and Phoa[22] have studied the influence of temperature on interfacial debonding on composites with TP-coated carbon fibers. In the late eighties, the elevated-temperature dependence of fracture energy mechanisms of hybrid carbon-glass fiber reinforced epoxy composites was studied by Munro and Lai,[20] who concluded that the work of fracture increased with temperature and glass fiber content. Indeed, the post-debond friction energy term was shown to be dominant, resulting from an extensive frictional work of the post-debond sliding type after glass fiber failure, in addition to that from the glass-fiber pull-out mechanism. Besides, the reinforcement architecture (UD or woven fabrics) also appears to significantly influence the extrinsic toughness of PMCs.[23,24] The influence of temperature on the interlaminar fracture toughness of TP-based composites was widely investigated in unidirectional composites as reviewed in previous studies,[7,8] and more specifically in the case of woven-ply laminates.[7,22] However, to the authors' best knowledge, there are no references dealing with the influence of temperature on translaminar failure.

This study deals with the fracture mechanics of hybrid laminated composites consisting of highly ductile TP matrix (polyether ether ketone (PEEK)) and brittle fibers. The effect of temperature and constraint effect on the strain energy release rate and crack extension of the laminates are specifically addressed in the case of a mode I translaminar failure mode. On the one hand, tests are carried out at room temperature (RT) and at 150°C (i.e. slightly higher than T_g as the ductile behavior of PEEK matrix is exacerbated) to examine the influence of temperature on fracture energy. On the other hand, tests are conducted on single-edge-notch tensile test (SENT) and single-edge-notch bending (SENB) specimens with different ratio a/w to investigate the influence of constraint effect on fracture toughness. The G-R curves were derived from the computation of the compliance loss and the crack extension in agreement with the ASTM standard E1820.

Table 1. A few properties of woven carbon and glass fibers reinforced PEEK elementary ply at RT.

	Carbon/PEEK	Glass/PEEK
E_x (GPa)	60	22
E_x (GPa)	60	20
G_{xy} (GPa)	4.8	6.55
v_{xy}	0.04	0.04
Tensile strength (warp) (MPa)	963	1172
Compressive strength (warp) (MPa)	725	1103
Nominal ply thickness (mm)	0.31	0.08
T_g (°C)	145	145

PEEK: polyether ether ketone; RT: room temperature.

Specimen description and test procedures

Materials

The laminated plates obtained by thermo-compression are made up of carbon (Tenax®-E HTA40 3K)–PEEK 5HS woven plies prepregs and glass–PEEK prepregs (Table 1). The consolidated laminates consist of 14 inner carbon-PEEK plies and two outer glass-PEEK plies.[25] The two outer glass-PEEK plies are considered for electrical protection purposes. In addition, the carbon and glass fiber fabrics are balanced in the warp and weft directions. The stacking sequence of laminates is quasi-isotropic (as shown in Figure 3): $[(0/90)_G,[(0/90),(\pm45)]_3,(0/90)]s$ (with G index for glass fibers ply). The average thickness of laminates is about 4.5 mm. The single-edge-notch test specimens (tensile and bending) were cut by water jet from $600 \times 600\,mm^2$ plates (Figure 4). The machining of the single-edge notches was done by means of a precision endless diamond wire saw whose radius was 0.085 mm. The initial notch length to specimen width ratio a/w ranges from 0.2 to 0.5 in both SENT and SENB specimens.

Methods and experimental set-up

Thermo-mechanical testing. All the tests were performed using a 100 kN capacity load cell of an MTS 810 servo-hydraulic testing machine in displacement-controlled

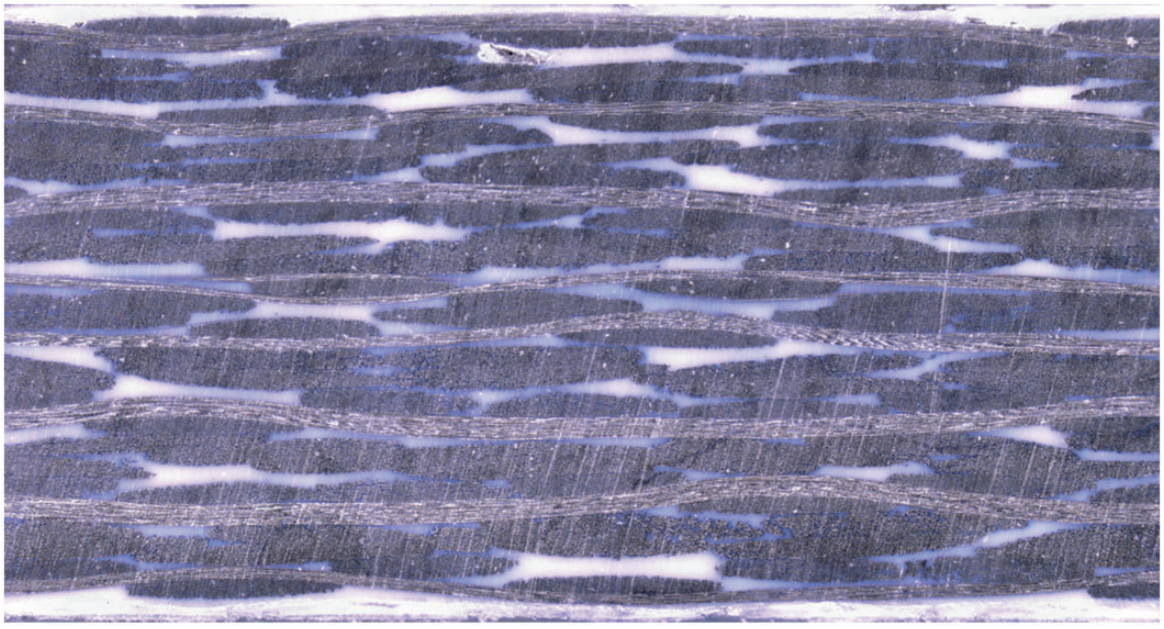

Figure 3. Optical micrograph of the longitudinal section revealing the quasi isotropic stacking sequence of the laminates.

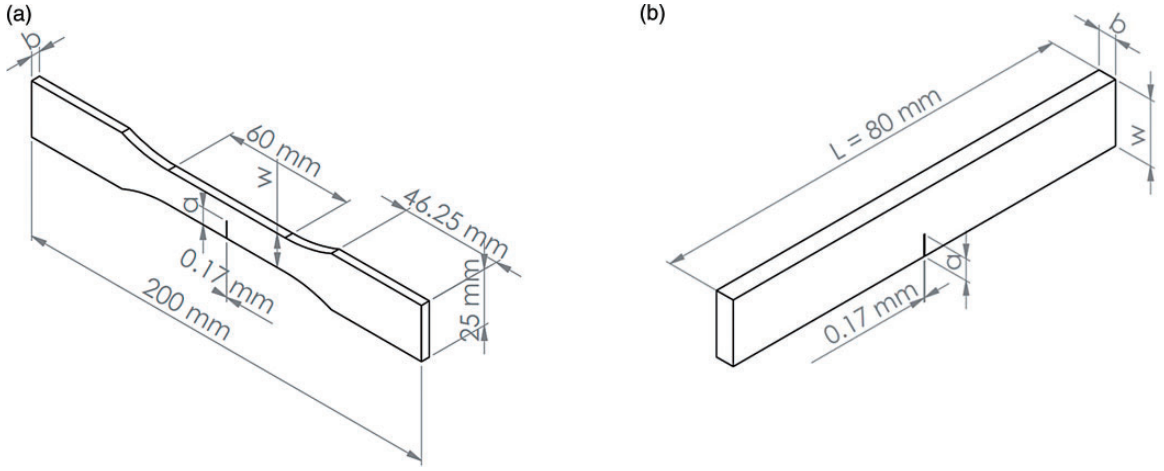

Figure 4. Geometry of single edge notched tensile specimens: (a) Tensile specimens and (b) bending specimens.

mode and with a temperature control system. Tensile and three-point bending loadings were applied to notched specimens at RT and 150°C.

Three specimens were tested in each configuration to obtain an acceptable average value. The tensile mechanical properties were determined according to the European standards EN 6035.[26] In SENT specimens, the longitudinal modulus (E_X) and ultimate strength (σ^u) were calculated from the following definitions

$$E_X = \frac{\Delta F}{S.\Delta\varepsilon_X} \quad \text{and} \quad \sigma^u = \frac{F^u}{S} \tag{1}$$

where ΔF is the difference in the applied tensile loads at $(\varepsilon_X)_2 = 0.25\%$ and $(\varepsilon_X)_1 = 0.05\%$,

S is the specimen cross section,

$\Delta\varepsilon_X = (\varepsilon_X)_2 - (\varepsilon_X)_1$ is the difference in the longitudinal strains obtained from a blade-extensometer,

F^u is the maximum force borne by the specimen at failure.

The mechanical properties of C/PEEK and G/PEEK elementary plies are specified in Table 1.[25]

The mechanical properties in bending were determined according to the European standards EN

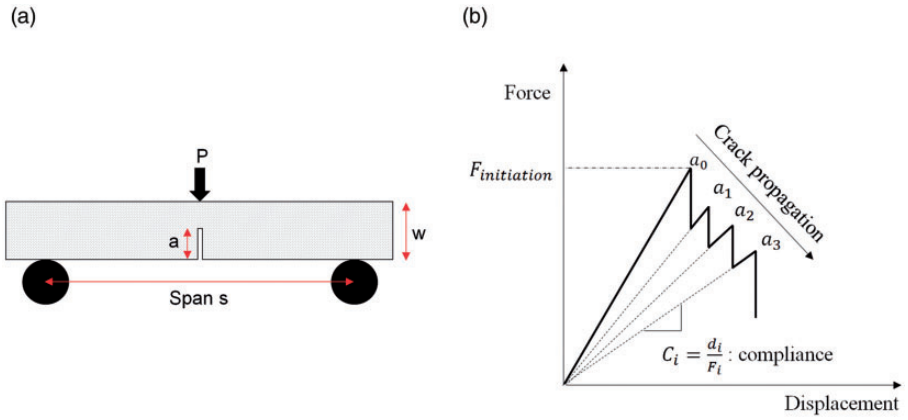

Figure 5. Estimation of the crack growth according to the ASTM standard E1820 test method applied to SENB specimens: (a) Dimensions and loading conditions and (b) crack growth vs compliance.

2562.[27] The bending strain and stress are defined as follows

$$\varepsilon_{bending} = \frac{6dw}{s^2} \quad \text{and} \quad \sigma_{bending} = \frac{3Ps}{2bw^2} \tag{2}$$

where b is specimen's thickness, s is the span between the support points, and d is the displacement applied to the upper part of the specimen (Figure 5(a)).

The bending stiffness is classically given by

$$E_{bending} = \frac{P^u s^3}{10bw^3(d_1 - d_2)} \tag{3}$$

where P^u is the ultimate load, d_1 and d_2 are the applied displacement at $P^u/2$ and $P^u/10$, respectively.

Relationship between fracture toughness and strain energy release rate. In orthotropic materials, the strain energy release rate G_I is classically obtained from the stress intensity factor K_I and the engineering constants[28]

$$G_{Ic} = C_I.K_{Ic}^2 \tag{4}$$

with $C_I = \sqrt{\frac{1}{2E_xE_y}}\sqrt{\sqrt{\frac{E_x}{E_y}} - \nu_{xy} + \frac{E_x}{2G_{xy}}}$ for plane stress conditions.

Let us recall that the coefficient C_I is simply given by $C_I = 1/E$ (E being the Young modulus) in the case of isotropic materials. The estimation of the fracture toughness depends on the geometry, the loading conditions and the characteristic length of the initial notch machined in the specimen to initiate failure.[29] The most commonly used specimens are SENB and SENT. The ASTM standard E1820 test method covers procedures and guidelines for the determination of fracture toughness of isotropic materials using the following parameters:[30] K, J, and crack tip opening displacement (CTOD). The fracture toughness determined in accordance with this test method is for the opening mode (mode I) of loading. The studied composite material has a quasi-isotropic behavior. To a first approximation, this method was applied to evaluate the mode I strain energy release rate from SENT and SENB specimens, as well as the crack growth in SENB specimens.

SENT specimens. The use of stress intensity factor values in engineering applications of fracture mechanics do not require values computed with absolute precision. Different approximations were proposed for K_I in the literature,[31] and the stress intensity factor is classically estimated by analytical functions in SEN specimens in mode I

$$K_I = \sigma\sqrt{\pi a}.F(a/w) \tag{5}$$

where σ is the remote applied stress, a denotes the length of the initial crack, and w is the specimen width (Figure 6). $F(a/w)$ is a geometric finite-width-correction (FWC) function calculated from the ratio a/w and empirical formulas. By definition, this FWC function is a scale factor applied to multiply the notched infinite-plate solution to obtain the notched finite-plate result.[32] For example, Gross and Srawley[33] have proposed the following expression in SENT specimens, whose precision is 0.5% for $a/w \leq 0.6$

$$F(a/w) = 1.122 - 0.231 * (a/w) + 10.550 * (a/w)^2 - 21.710 * (a/w)^3 + 30.382 * (a/w)^4 \tag{6}$$

SENB specimens. As introduced in the case of SENT specimens, the mode I fracture toughness is also estimated from the equation (5). The geometric

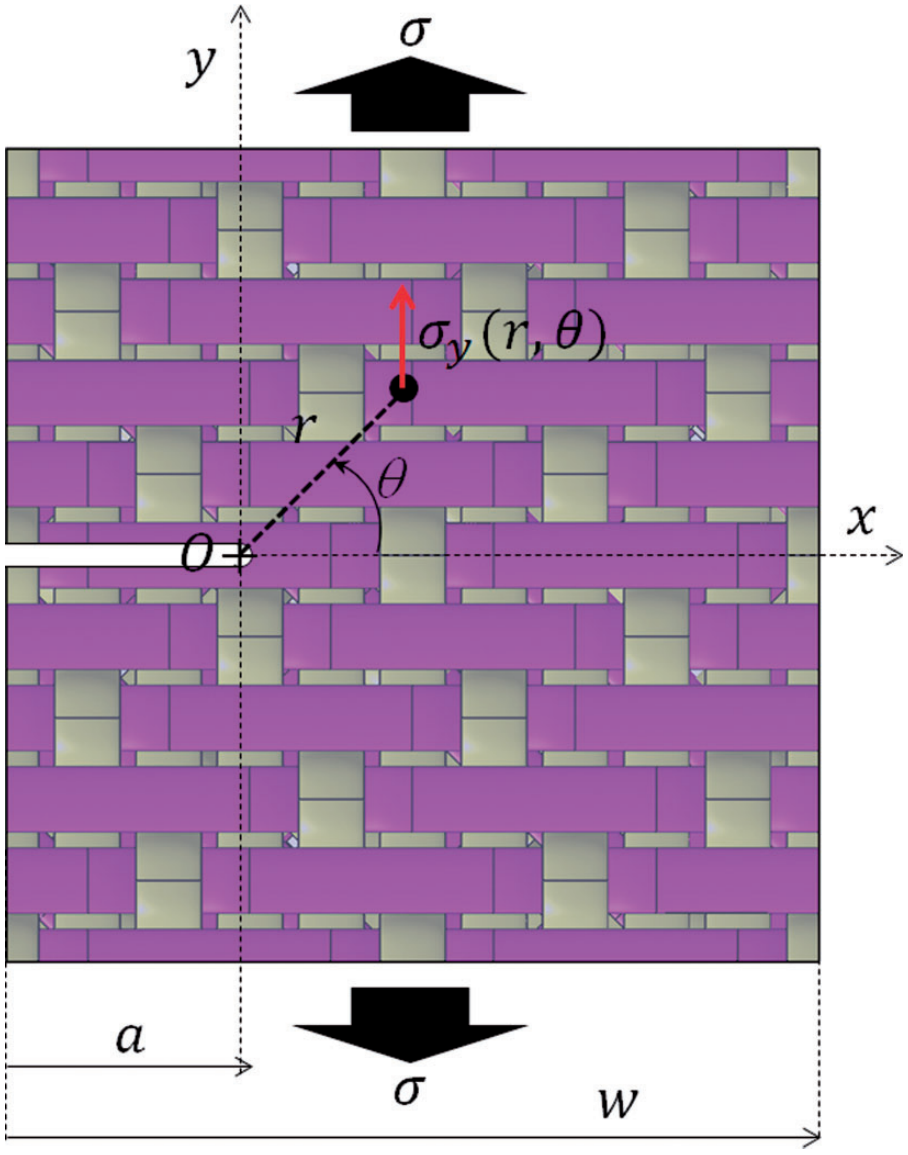

Figure 6. Longitudinal stress in the vicinity of the crack tip in QI SEN laminates loaded in mode I.

finite-width-correction function $F(a/w)$ is calculated from the ratio a/w and empirical formulas whose precision is 0.5% for any ratio a/w[31]

$$F(a/w) = \frac{1}{\sqrt{\pi}} \cdot \frac{[1.99 - (a/w)(1 - a/w)(2.15 - 3.93 * \frac{a}{w} + 2.7 * (a/w)^2]}{(1 + 2 * a/w)(1 - a/w)^{3/2}} \quad (7)$$

In SENB specimens, the ASTM standard E1820 test method gives an estimation of the crack growth versus applied stress.[30] Thus, the crack length on an SENB specimen is normally determined from crack opening compliance. According to the ASTM standard, it is determined from load-line compliance if the correct calibration is available. For a resistance curve test method using an elastic compliance technique (Figure 5(b)) on single-edge bend specimens with crack opening displacements measured at the notched edge, the crack length a_i is given as follows

$$a_i/w = [0.999748 - 3.9504u + 2.9821u^2 - 3.21408u^3 + 51.51564u^4 - 113.031u^5] \quad (8)$$

where $u = \frac{1}{\left[\frac{BWEC_i}{S/4}\right]^{1/2} + 1}$

and B and W are the specimen thickness and width, respectively,

E is the longitudinal stiffness,

$C_i = (\Delta v_m/\Delta P)$ is the crack opening compliance (the ratio of displacement increment to load increment)

obtained from the crack opening displacement at notched edge v_m and the applied load P,

S is the specimen span, the distance between specimen supports (Figure 5(a)).

Finally, the expression of σ_y at the crack tip (Figure 6) is used to estimate the stress concentration factor K_T for mode-I type loading[29]

$$K_T = \frac{\sigma_y(\theta = 0)|_{x=0}}{\sigma} = \sqrt{\frac{a}{2r}}.F(a/w) \quad (9)$$

where $r = 0.085$ mm is the radius of the notch at the crack tip and σ is the remote applied stress far from the notch.

Fractographic analyses. Damage mechanisms are discussed by means of fractographic analyses: macroscopic observations with a Keyence optical microscope and tomographic observations with a Microtomograph Easytom 130 supplied by the company RX Solutions.

Results and discussion

Macroscopic mechanical response and fracture behavior

From the macroscopic response standpoint, both SENT and SENB specimens exhibit a brittle failure at RT with a tendency to shift towards a quasi-brittle failure (Figures 7 and 8) as the initial notch length-to-specimen width ratio a/w (typically from 0 to 0.5) and test temperature increase. As the ratio a/w increases, the stress concentration factor computed from equations (6, 7, 9) gradually increases at the crack tip (Figure 9). In SENT specimens, the influence of stress concentration is about the same with an 80% decrease in the

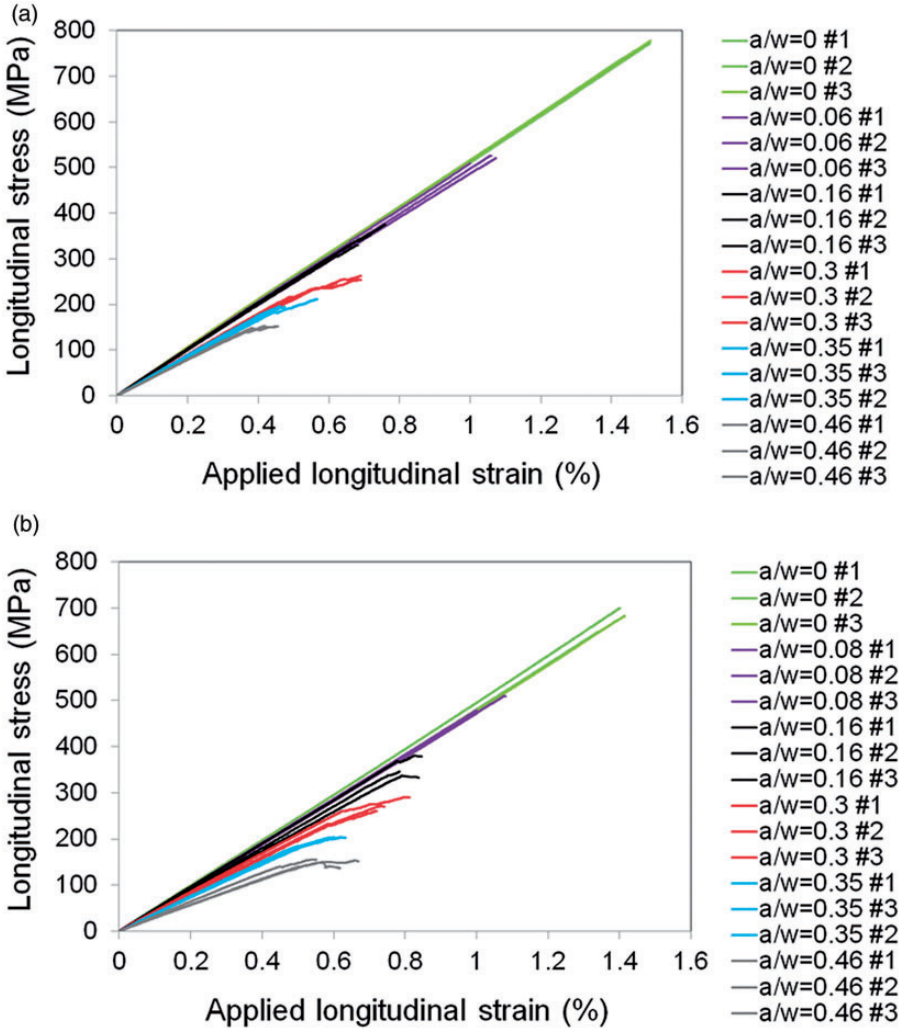

Figure 7. Constraint effect on SENT specimens: (a) RT and (b) 150°C.
SENT: single edge notch tensile; RT: room temperature.

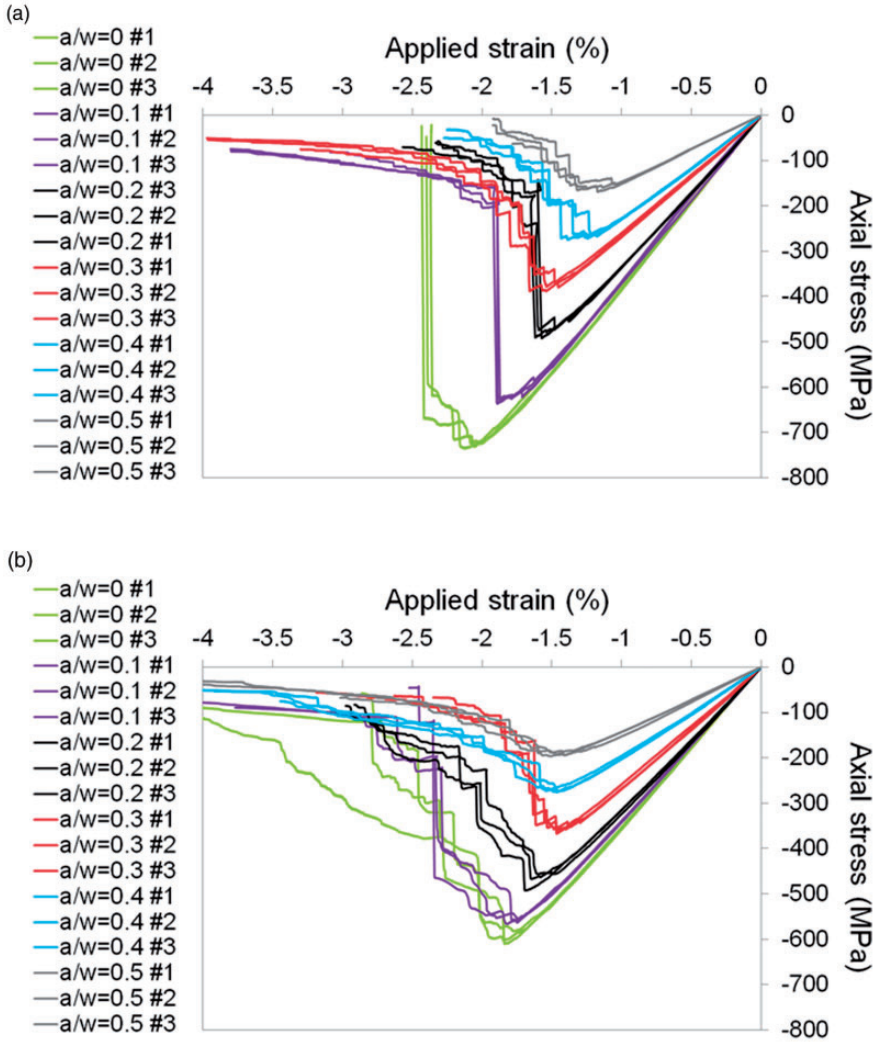

Figure 8. Constraint effect on SENB specimens: (a) RT and (b) 150°C.
SENB: single edge notch bending; RT: room temperature.

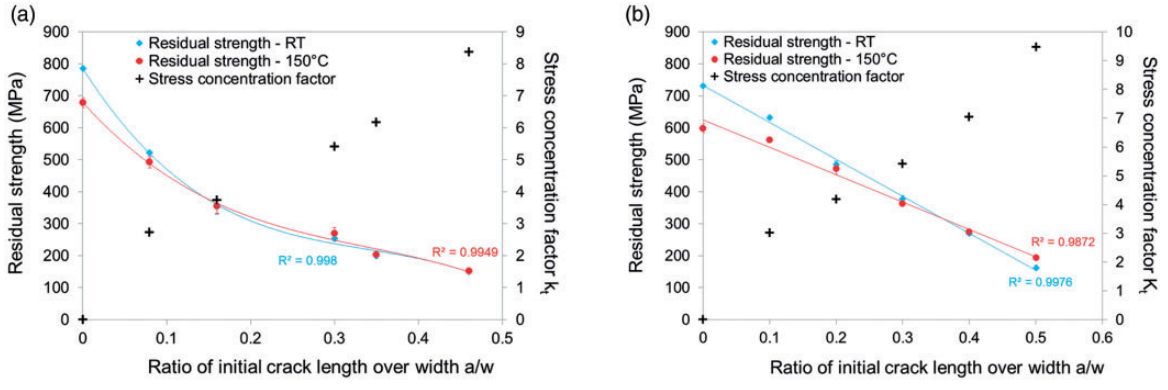

Figure 9. Influence of temperature and constraint effect (quantified by the stress concentration factor) on the residual strength of QI laminates: (a) SENT and (b) SENB.
SENT: single edge notch tensile; SENB: single edge notch bending.

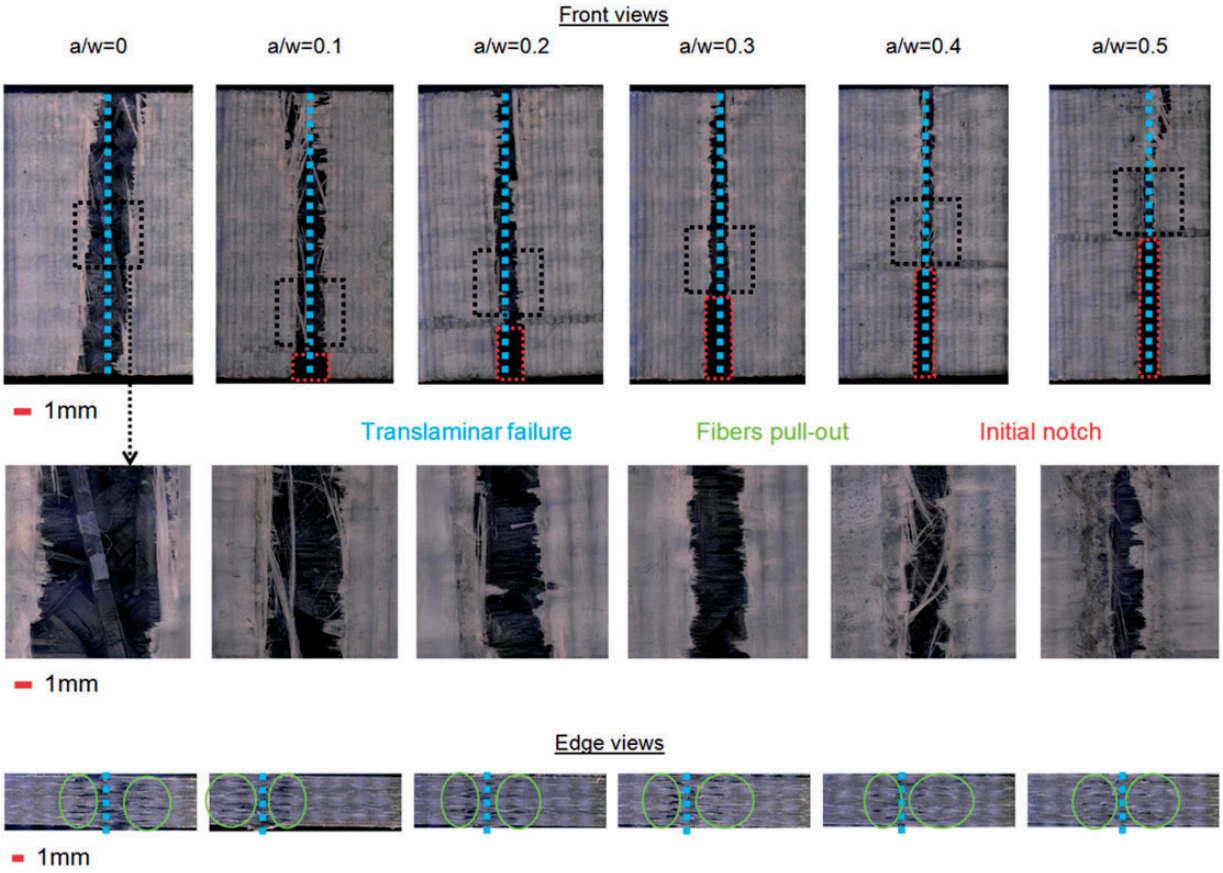

Figure 10. Microscopic observations of SENT specimens after failure in mode I at 150°C.
SENT: single edge notch tensile.

residual strength at both temperatures (Figure 9(a)). In SENB specimens, the constraint effect (quantified by the stress concentration factor K_t) decreases the residual strength by virtually 80% and 70% at RT and 150°C, respectively (Figure 9(b)). In both SENT and SENB specimens, the influence of temperature on the residual strength is limited. The decrease in the residual strength along with an increasing a/w ratio appears to be hyperbolic in SENT specimens and linear in SENB specimens.

In both SENT and SENB specimens, the microscopic observations of failure surfaces clearly show that fracture is translaminar in mode I loading even at elevated temperature (Figures 10 and 11) regardless of the a/w ratio. At RT, translaminar fracture is observed in all specimens. The front views indicate that the macroscopic translaminar macroscopic crack grows self-similarly with respect to the initial notch in SENT specimens. In SENB specimens with low a/w ratio, the translaminar crack is not self-similar.

In SENT specimens, failure is primarily dominated by the tensile breakage of 0° carbon fibers, with no visible contribution of the +/−45° plies suggesting that the quasi-brittle failure observed at 150°C is primarily resulting from some fiber/matrix debonding coming along with fibers pull-out (edge views Figure 10).

In SENB specimens, failure consists of tensile and compressive breakage of 0° carbon fibers particularly in specimens with low a/w ratio (Figure 11). When loaded in bending, the upper part of specimens (above the neutral axis) is subjected to compression whereas the lower part (below the neutral axis) is subjected to tension. In addition, local crushing of the upper edges is observed in the contact area. As a/w ratio increases (typically from $a/w = 0.3$), the stress concentration factor K_t increases as well (Figure 9(b)), and promotes a translaminar failure dominated by the tensile breakage of 0° carbon fibers. No visible damage is observed on upper edges of these specimens as the bending stress is lower than the crushing stress.[25] The gradual failure observed at 150°C is primarily associated with glass fibers bridging at the outer surfaces of specimens (Figure 12). The ultimate strength of G/PEEK plies being lower than C/PEEK plies, glass fibers cannot take up the load transferred to neighboring fibers when carbon fibers fail. Thus, glass fiber bridging results from the debonding at the glass fiber/matrix interface as is observed on

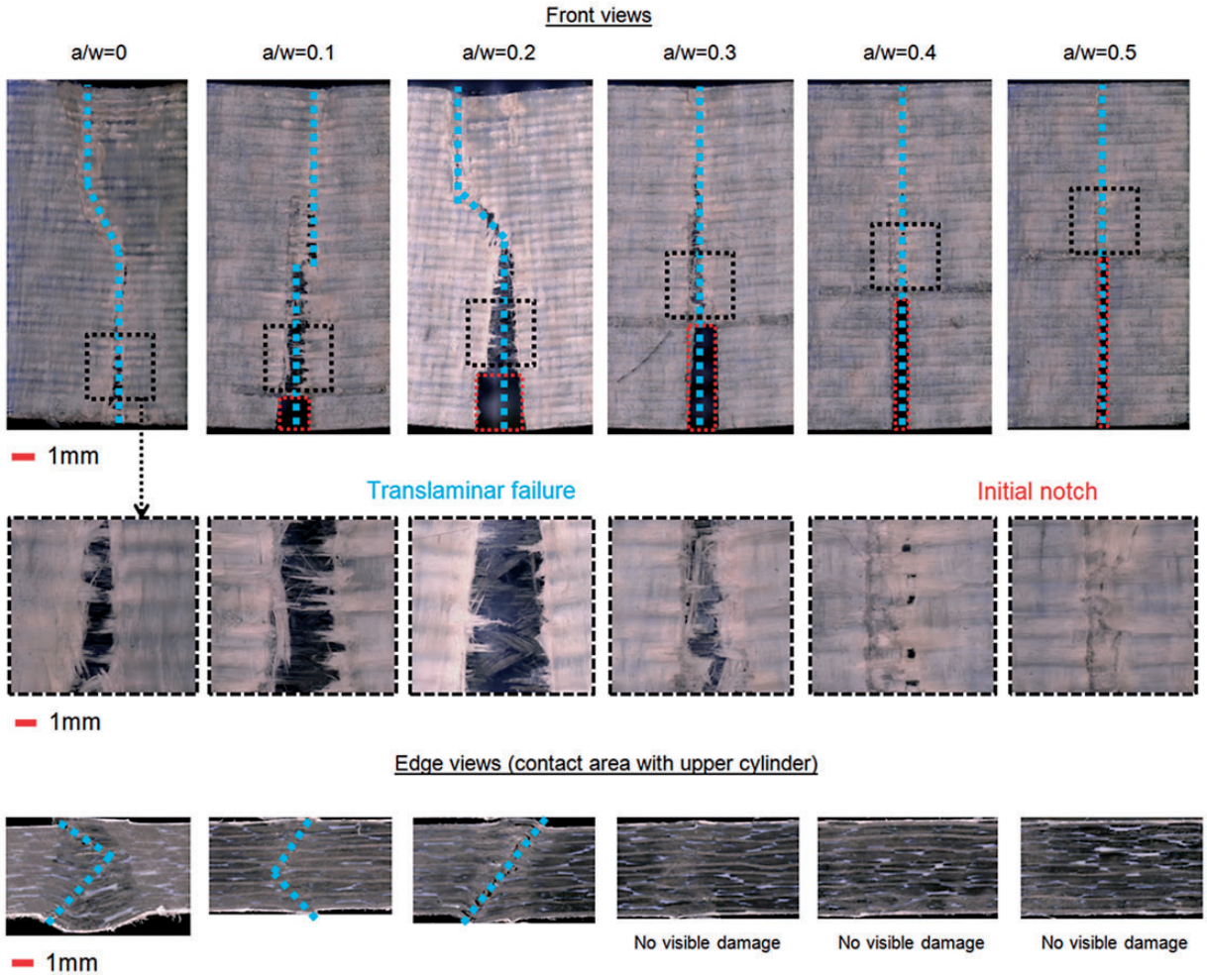

Figure 11. Microscopic observations of SENB specimens after failure in mode I at 150°C.
SENB: single edge notch bending.

the microscopic observation. As carbon fibers breakage comes along with the crack mouth opening, gradual glass fibers pull-out may be observed behind the crack tip. In addition, temperature promotes local crushing (resulting from compression) in the contact area, and exacerbates ductility at $T > T_g$.[11,15] It therefore contributes to the retardation of the crack extension and the increase in the fracture toughness as will be further discussed in section "Influence of constraint effect on G-R curves".

Influence of temperature on G-R curves

Depending on the specimen's geometry and the loading mode, fiber-reinforced composites are generally characterized by an observable stable crack growth before instability,[34] and the fracture toughness (or critical strain energy release rate) usually increases with crack extension before reaching a plateau value (Figure 13). Thus, the critical fracture toughness Kc is not sufficient to characterize the whole fracture behavior and the concept of crack resistance curves (described as G-R curves) has to be adopted.[35] Within the framework of LEFM, the determination of G-R curves is therefore the key point to quantify fracture in terms of energy required to grow a crack in quasi-isotropic laminates. In the present work, the idea was first to build equivalent G-R curves based on the evaluation of fracture toughness for different ratios a/w and different loadings (e.g. tensile and bending). From equations (5–7), it is possible to compute the value of the critical fracture toughness K_{Ic} in SENT and SENB specimens (Figure 14). As failure is primarily driven by carbon fibers breakage in tension (SENT) and in tension/compression (SENB), it turns out that a temperature increase has very little influence on the critical translaminar fracture toughness though the ductility of PEEK matrix is exacerbated at $T > T_g$. It also appears that the constraint effect has very little influence on the critical mode I fracture energy as SENT and SENB specimens

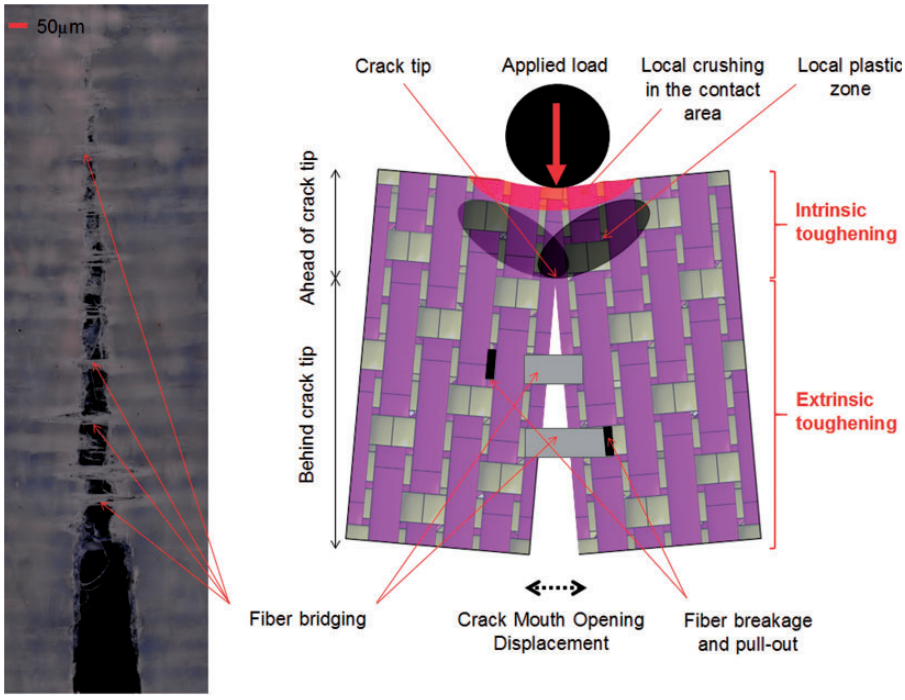

Figure 12. Illustration of crack extension and crack mouth opening displacement in SENB specimens at 150°C (a/w 0.3): influence of fiber bridging on extrinsic toughness.
SENB: single edge notch bending.

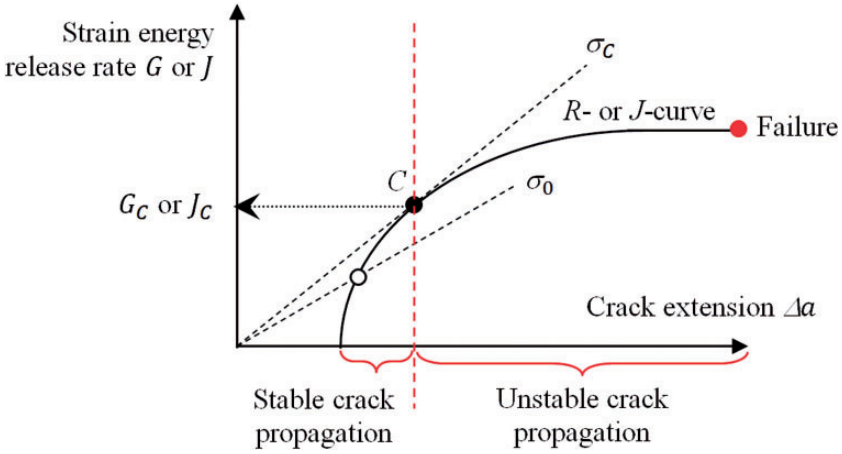

Figure 13. Determination of the critical fracture toughness from R or J curves.[16]

have virtually the same mean value (about 45MPa. $\sqrt{m}$). With increasing ratio a/w, the strain energy release rate increases gradually in SENT specimens (Figure 14(a)), whereas it slowly increases and gradually decreases in SENB specimens, resulting from less contribution of compressive failure (Figure 14(b)).

According to equation (8), the crack length a_i is computed from the crack opening compliance as described in ASTM standard E1820. Thus, the critical strain energy release rate in opening mode G_{Ic} is classically obtained from the load-line compliance $C = d/P$ and the crack length (Figure 5(b))[29]

$$G_I = \frac{P^2}{2B}\frac{dC}{da} \tag{10}$$

where d represents the applied displacement, P the force borne by the specimen, and B is the specimen width.

The G-R curves are drawn from this expression and the translaminar crack extension (Figure 15). This

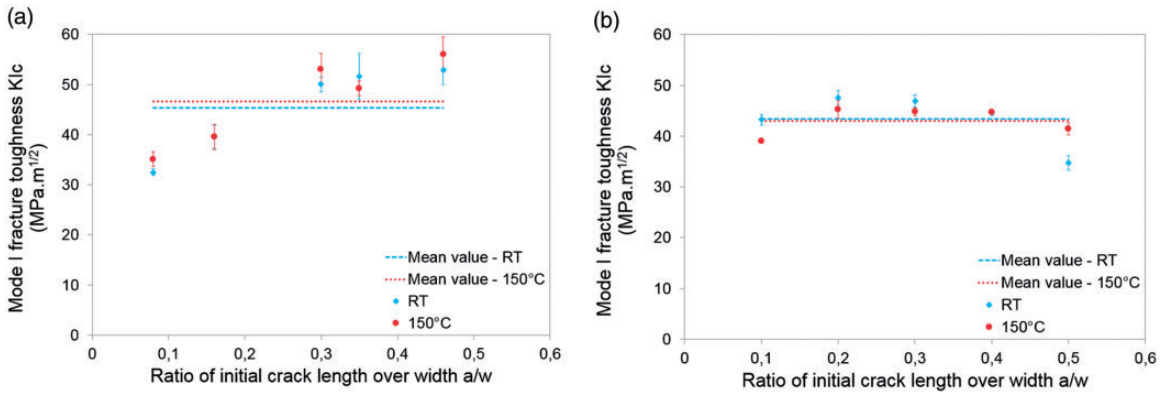

Figure 14. Influence of temperature and constraint effect on the mode I fracture translaminar toughness of QI laminates: (a) SENT and (b) SENB. SENT: single edge notch tensile;
SENB: single edge notch bending.

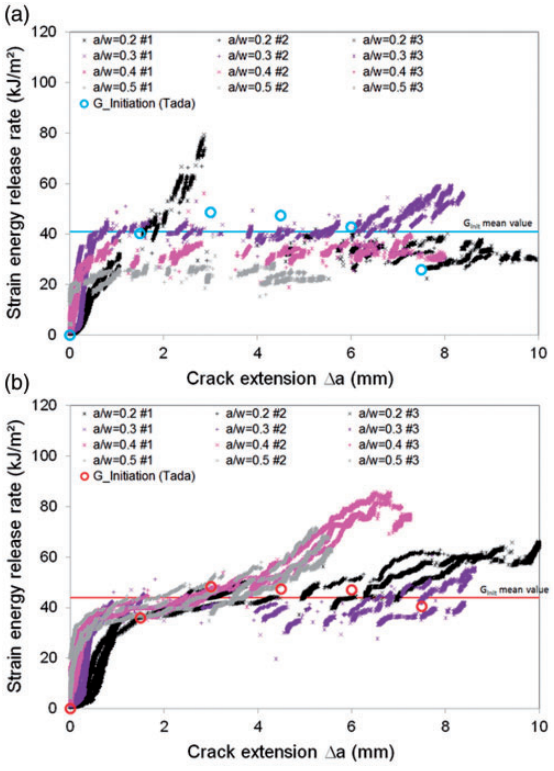

Figure 15. Evolution of strain energy release rate along with the crack growth in SENB specimens with different ratio a/w: (a) RT – (b) 150°C.
SENB: single edge notch bending; RT: room temperature.

technique was applied to the tests conducted at both temperatures. As will be discussed in section "Translaminar failure in SENB specimens," the gradual failure observed at high temperature is associated with glass fiber bridging. This contributes to the increase in the extrinsic toughness, hence slowing down the crack extension (Figure 12). The equivalent

Table 2. Mechanical properties of the equivalent orthotropic material – Quasi isotropic CG/PEEK laminates.

	E_x (GPa)	E_x (GPa)	G_{xy} (GPa)	v_{xy}	$C_1\,(GPa^{-1})$
RT	49.58	49.58	15.76	0.289	0.0215
150°C	45.55	45.55	14.48	0.266	0.0236

PEEK: polyether ether ketone; RT: room temperature.

G-R curves built from equation (4) and the fracture toughness at crack initiation K_I corresponding to different ratio a/w (Figure 14) are reported in Figure 15 in terms of strain-energy release rate in both test temperatures. It is therefore possible to compare the evolution of the strain energy release vs crack propagation with the values of $G_{I\,init}$ at crack initiation computed from different ratio a/w. The values at initiation computed from LEFM equations[31] are in agreement with the values obtained during propagation from the compliance loss (ASTM standard E1820). As indicated previously, a temperature increase to temperatures higher than T_g has little influence on the translaminar fracture toughness, and the mean value of G_{Ic} (computed from equation (4)) slightly increases at 150°C (from 41 kJ/m^2 to 44 kJ/m^2, hence a 7% increase) because the mechanical properties of the equivalent orthotropic material slightly change between RT and 150°C resulting from the softening of the PEEK matrix (Table 2).

Influence of constraint effect on G-R curves

In PMCs, Allaer et al.[36] have studied the influence of the constraint effect during fracture toughness tests by means of SENB specimens in order to define a valid plane strain fracture toughness value K_{Ic}. The influence of crack tip constraint effect (depending on the specimen geometries and the loading conditions) and stress

triaxiality (depending on the initial notch length to specimen width ratio a/w) on ductile and brittle fracture is of major importance for the assessment of structural integrity. The loss of constraint effect is related to the position and the size of the plastic zones. Indeed, the deeper the notch and the higher the test temperature, the greater are the plastic zone and constraints (resulting from the triaxial stress state). Therefore, the higher the loading force must be to deform the sample.[2] As a consequence, it is usually observed that the decrease in crack tip constraint (the stress concentration at the notch root is offset by plastic deformation) leads to an increase of the fracture toughness (corresponding to a ductile failure).

Translaminar failure in SENB specimens

As pointed in section "Macroscopic mechanical response and fracture behaviour," the fracture mechanisms are modified at $T > T_g$ because of glass fiber bridging behind the crack tip and local plastic deformation in matrix-rich areas ahead of the crack tip as translaminar crack grows (Figure 12). It appears that both mechanisms are enhanced when matrix ductility increases. Indeed, instead of the sudden breakage of 0° carbon fibers at RT, the ductile behavior of the PEEK matrix at the fiber/matrix interface contributes to the dissipation of a portion of the mechanical energy during the load transfer between a broken fiber bundle and the neighbor fibers.

In order to investigate more specifically the contribution of the 0° and +/-45° oriented plies in quasi-isotropic CG/PEEK laminates, X-ray tomographic observations were conducted in SENB specimens with a ratio $a/w = 0.3$ (Figure 16). In 0° plies, a clear translaminar crack is observed suggesting the catastrophic failure of 0° carbon fiber bundles initiated from the stress concentration in the vicinity of the initial notch. A local crushing (or compressive failure) of laminates' upper edges in the contact area with the upper cylinder is also observed. In +/-45° oriented plies, the fracture surface reveals the breakage of +/−45° carbon fibers in shearing. In QI laminates, the macroscopic failure is primarily dominated by 0° fibers, resulting in a virtually temperature-independent behavior (even at $T > T_g$) as the +/−45° oriented plies do not significantly contribute to bear the mechanical loading. From the fracture mechanics standpoint, the translaminar failure is initiated when the stress intensity factor in tension reaches its critical value $K_{Ic}^{tension}$.

A brittle interface allows crack advance by sudden breakage of 0° carbon fibers, while a ductile interface forms a well-defined glass fiber-bridged crack potentially leading to divert the crack front and to reduce crack growth.[34] After the failure of carbon fibers, the broken glass fiber locally debonds from the matrix, and the matrix surrounding the broken fiber ends is stressed at a significantly higher level than prior to the fiber failure. The resulting temporary and local plastic deformation of the matrix in this area comes along with a gradual pull-out of 0° glass fibers at 150°C as the translaminar macroscopic crack grows, therefore leading to glass fiber-bridging that reduces the crack mouth opening. At RT, pull-out is reduced as sudden breakage of 0° carbon fibers does not allow the matrix to dissipate the mechanical energy by means of

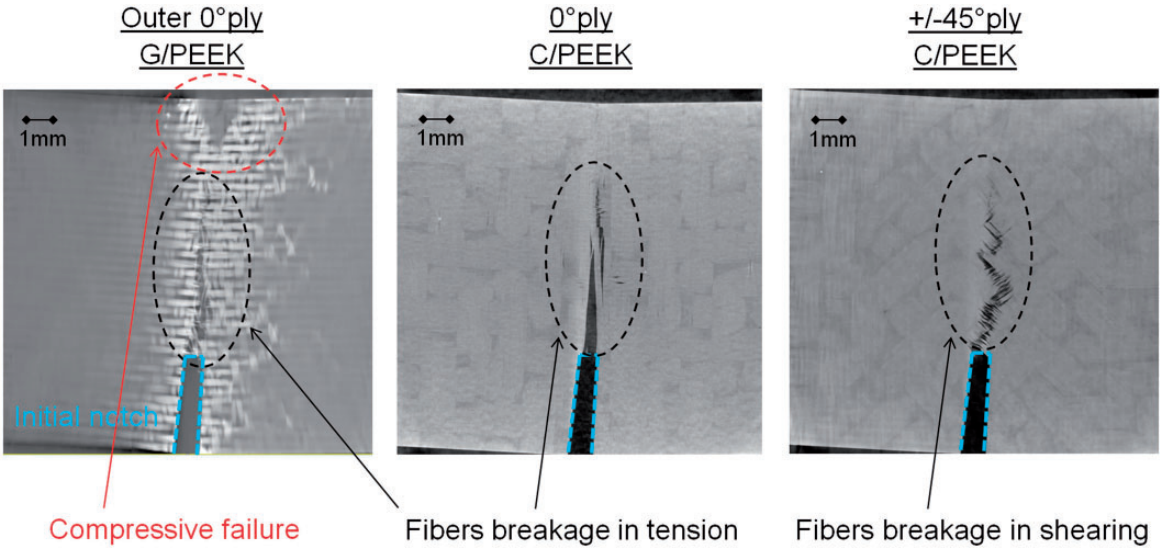

Figure 16. Tomographic observations of SENB specimens (a/w 0.3) at 150°C.
SENB: single edge notch bending.

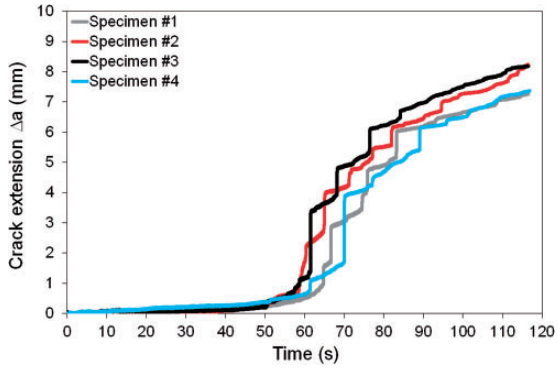

Figure 17. Evolution of the crack growth estimated by the ASTM standard E1820 test method applied to SENB specimens (a/w 0.3) at 150°C.
SENB: single edge notch bending.

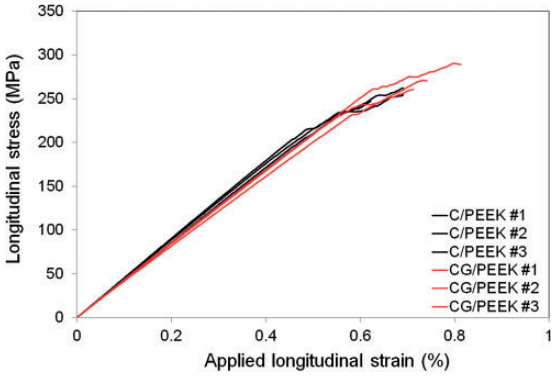

Figure 18. Influence of outer glass fibers/PEEK laminates on the tensile response of SENT specimens (a/w 0.3) at 150°C.
SENT: single edge notch tensile.

inelastic deformation and does not imply significant interface debonding in the outer G/PEEK plies. These mechanisms are instrumental in ruling the mechanical energy released during fracture. More specifically, the strain energy release rate increases at macroscopic scale resulting from enhanced ductility of the PEEK matrix at microscopic and mesoscopic scales as temperature increases. In addition, a larger number of glass fibers bridge the crack as it grows. Ultimately, such fiber-bridging results in increasing the mode I translaminar toughness during the last stage of fracture.

Influence of glass fibers on extrinsic toughness

SENB specimens are characterized by a gradual failure (particularly at 150°C as explained in section "Translaminar failure in SENB specimens"). G-R curves were derived from equation (10) and the corresponding gradual crack growth in agreement with the ASTM standard E1820. It is therefore possible to observe a sigmoid evolution of crack extension vs time (Figure 17). Until crack initiation at maximum stress (about 350 MPa for a 1.7% axial strain), the crack length is virtually unchanged. Therefore, it suddenly increases and jumps are clearly observed on the curves obtained from the ASTM method. These jumps are associated with the breakage of 0° carbon fibers. The stress redistribution to the neighboring fibers was described in details in section "Translaminar failure in SENB specimens". Both glass fiber bridging and local plastic deformation of the PEEK matrix at the interface and at the crack tip contributes to the momentary stabilization of the crack growth. At the end of loading, when the stress borne by specimens tends to low values (typically less than 100 MPa as shown on Figure 8(b)), it appears that there are no jumps (because all the 0° fibers are broken), and the crack extension gradually slows down as there are lots of bridged glass fibers behind the crack tip reducing the crack mouth opening (microscopic observations on the left on Figure 12). Thus, the fracture process zone consists of two zones (behind and ahead of the crack tip) resulting from the damage mechanisms taking place during translaminar cracking:[35,37]

1. The damage zone ahead of the advancing crack tip where matrix cracking, interfacial debonding, and post-debonding friction occurs;
2. The glass fibers bridging zone or tied zone at the wake of the crack tip where glass fibers bridge the opposite fracture surfaces and pull-out.

These two zones are closely associated with both intrinsic and extrinsic fracture toughness. In the present case, the highly ductile behavior of the PEEK matrix at $T > T_g$ provides good intrinsic toughness to quasi-isotropic hybrid laminates, whereas the bridging of macroscopic translaminar crack by the glass fibers at the outer surfaces of laminates contributes to the increase in its extrinsic toughness. This evolution of the G-R curve is in agreement with the observations proposed in previous studies:[3 5,20,37] extrinsic toughness primarily contributes to the increase in the fracture energy during crack growth by means of crack-tip shielding mechanisms that result in rising R-curve behavior.

The purpose of the present work was not to specifically address the influence of hybridization on fracture toughness (it will be investigated in a forthcoming paper). However, the effect of the extrinsic toughening by the glass fibers is indeed expected to be small. For quantification purposes, the extrinsic toughening by the glass fibers is evaluated from tests on SENT specimens (with a ratio $a/w = 0.3$) consisting of carbon fiber reinforced PEEK matrix laminated composites on the one hand and glass and carbon fiber reinforced PEEK

matrix composites on the other hand (Figure 18). From the macroscopic mechanical standpoint, the outer glass fiber PEEK plies have a moderate influence. From these tests, the mode I fracture toughness is evaluated by equations (5) and (6). The results suggest that glass fibers virtually do not influence K_{Ic} as it increases from 50.04 to 53.06 MPa. $\sqrt{}$m (hence a 6% increase) in C/PEEK and CG/PEEK laminates, respectively.

Conclusions

Tensile and bending tests were conducted at RT and 150°C ($T > T_g$) on single-edge notched specimens consisting of hybrid carbon glass reinforced PEEK composite materials. In the studied quasi-isotropic laminates, the translaminar crack is dominated by the breakage of 0° carbon fibers, and appears to be self-similar in both SENT and SENB specimens.

Equivalent G-R curves are obtained from SENT and SENB specimens with different initial notch length to specimen width ratio a/w (typically from 0 to 0.5). As failure is primarily driven by carbon fibers breakage in tension (SENT) and in tension/compression (SENB), it turns out that a temperature increase has very little influence on the mode I critical translaminar fracture toughness K_{Ic} though the ductility of PEEK matrix is exacerbated at $T > T_g$. It also appears that the constraint effect has very little influence on K_{Ic} as SENT and SENB specimens have virtually the same mean value (about 45 MPa. $\sqrt{}$m).

G-R curves were derived from the computation of crack growth and compliance loss in agreement with the ASTM standard E1820. After reaching a plateau value, the critical strain energy release rate in mode I gradually increases as the translaminar crack ultimately grows. The late increase in translaminar toughness results from both intrinsic and extrinsic toughness that are specifically enhanced at $T > T_g$. The fracture energy is associated with the brittle failure of carbon fibers leading to gradual fiber bridging of glass fibers (contributing to a reduced extrinsic toughness), whereas the highly ductile PEEK matrix provides the composite material its intrinsic toughness by means of local plastic deformation at the crack tip and around the broken fibers ends.

Declaration of Conflicting Interests

The author(s) declared no potential conflicts of interest with respect to the research, authorship, and/or publication of this article.

Funding

The author(s) received no financial support for the research, authorship, and/or publication of this article.

ORCID iD

B Vieille http://orcid.org/0000 0003 4528 7167

References

1. Ritchie RO. Mechanisms of fatigue crack propagation in ductile and brittle solids. *Int J Fract* 1999; 100: 55 83.
2. Hertzberg RW, Vinci RP and Hertzberg JL. Element of fracture mechanics. In: Hertzberg RW (ed.) *Deformation and fracture mechanics of engineering materials*, 5th ed. Hoboken, USA: Wiley & Sons, 1996.
3. Launey ME and Ritchie RO. On the fracture toughness of advanced materials. *Adv Mater* 2009; 21: 2103 2110.
4. Tardiff G. Fracture mechanics of brittle matrix ductile fiber composites. *Eng Fract Mech* 1973; 5: 1 10.
5. Naerheim Y. Fracture characteristics of a ductile matrix/brittle fiber composite. *Metall Transact A* 1976; 7: 63 70.
6. Kim JK and Mai YW. The effect of interfacial coating and temperature on the fracture behaviours of unidirec tional KFRP and CFRP. *J Mater Sci* 1991; 26: 4701 4720.
7. Fracasso R, Rink M, Pavan A, et al. The effects of strain rate and temperature on the interlaminar fracture tough ness of interleaved PEEK/CF composites. *Compos Sci Technol* 2001; 61: 57 63.
8. Jacob GC, Starbuck JM, Fellers JF, et al. The effect of loading rate on the fracture toughness of fiber reinforced polymer composites. *J Appl Polymer Sci* 2005; 96: 899 904.
9. Kassapoglou C. *Modeling the effect of damage in compos ite structures: simplified approaches*, 1st ed. Chichester, UK: John Wiley & Sons Ltd, 2015, pp.41 56.
10. Laffan MJ, Pinho ST, Robinson P, et al. Translaminar fracture toughness testing of composites: a review. *Polym Test* 2012; 31: 481 489.
11. Vieille B. Evolution of the strain energy release rate during ductile or brittle failure in woven ply reinforced thermoplastic laminates under high temperature condi tions. *Polym Compos* 2018. DOI: 10.1002/pc.24612.
12. Reifsnider KL. Damage and damage mechanics. In: Reifsnider KL (ed.) *Fatigue of composite materials*. Amsterdam, The Netherlands: Elsevier Science Publishers BV, 1990, pp.11 78.
13. Jones RM. Other analysis and behavior topics. In: *Mechanics of composite materials*, 2nd ed. London, UK: Taylor & Francis, 1999, p.345.
14. Harris B. A historical review of the fatigue behavior of fiber reinforced plastics. In: Harris B (ed.) *Fatigue in com posites science and technology of the fatigue response of fiber reinforced plastics*. Woodhead Publishing, 2003, pp.3 35.
15. Wells JK and Beaumont PWR. Crack tip energy absorp tion processes in fibre composites. *J Mater Sci* 1985; 20: 2735 2749.
16. Vieille B, Chabchoub M, Bouscarrat D, et al. A fracture mechanics approach using acoustic emission technique to investigate damage evolution in woven ply thermoplastic structures at temperatures higher than glass transition temperature. *Compos B* 2017; 116: 340 351.

17. Vieille B, Chabchoub M and Gautrelet C. Influence of matrix ductility and toughness on strain energy release rate and failure behavior of woven ply reinforced thermo plastic structures at high temperature. *Compos B Eng* 2018; 132: 125 140.
18. Beaumont PWR. Physical modelling of damage develop ment in structural composite materials under stress. In: Harris B (ed.) *Fatigue in composites: science and tech nology of the fatigue response of fiber reinforced plastics*. Cambridge: Woodhead Publishing Ltd., 2003, pp.365 412.
19. Lauke B and Pompe W. Fracture toughness of short fibre reinforced thermoplastics. *Compos Sci Technol* 1986; 26: 37 57.
20. Munro M and Lai CPZ. The elevated temperature dependence of fracture energy mechanisms by hybrid carbon glass fiber reinforced composites. *J Mater Sci* 1988; 26: 4701 4720.
21. Wells JK and Beaumont PWR. The prediction of R curves and notched tensile strength for composite lamin ates. *J Mater Sci* 1987; 22: 1457 1468.
22. Kim K Y and Phoa K M. Interlaminar fracture tough ness of CF/PEI and GF/PEI composites at elevated tem peratures. *Appl Compos Mater* 2004; 11: 173 190.
23. Flore D, Stampfer B and Wegener K. Experimental and numerical failure analysis of notched quasi unidirectional laminates at room temperature and elevated temperature. *Compos Struct* 2017; 160: 128 141.
24. Ortega A, Maimí P, González EV, et al. Translaminar fracture toughness of interply hybrid laminates under ten sile and compressive loads. *Compos Sci Technol* 2017; 143: 1 12.
25. Dubary N, Taconet G, Bouvet C, et al. Influence of tem perature on the impact behavior and damage tolerance of hybrid woven ply thermoplastic laminates for aeronaut ical applications. *Compos Struct* 2017; 168: 663 674.
26. Test standard EN 6035, Aerospace series Fiber rein forced plastics Test Method Determination of notched and unnotched tensile strength. Published by the European Association of Aerospace Industries (AECMA), April 1996.
27. Test standard EN 2562, Aerospace series Carbon Fiber reinforced plastics Test Method Unidirectional lamin ates, flexural test parallel to the fiber direction. Published by the European Association of Aerospace Industries (AECMA), March1997.
28. Sih GC and Chen EP. Cracks in composite materials. In: Sih GC (ed.) *Mechanics of fracture*. Vol 6, London: Martinus Nijoff Publishers, 1981.
29. Vieille B, Chabchoub M, Bouscarrat D, et al. Prediction of the notched strength of woven ply polyphenylene sul fide thermoplastic composites at a constant high tempera ture by a physically based model. *Compos Struct* 2016; 153: 529 537.
30. ASTM standard E1820 test method. *Standard Test Method for Measurement of Fracture Toughness*. West Conshohocken, PA: ASTM International, 2018. DOI: 10.1520/E1820 18.
31. Tada H, Paris PC and Irwin GR. *The stress analysis of cracks handbook*, 3rd ed. New York, USA: ASME Press, 2000.
32. Tan SC. *Stress concentration in laminated composites*. Lancaster, PA: Technomic Pub. Co., 1994.
33. Gross B and Srawley JE. Stress intensity factors for single edge notch tension specimens by boundary collo cation of a stress function. NASA TN D 2395, 1964.
34. Talreja R. Fatigue damage mechanisms. In: Talreja R and Varna J (eds) *Modeling damage, fatigue and failure of composite materials*. Amsterdam: Elsevier, 2015.
35. Kim J K and Mai Y W. Interface mechanics and fracture toughness theories. In: Kim JK and Mai YW (eds) *Engineered interfaces in fiber reinforced composites*. Amsterdam: Elsevier, 1998.
36. Allaer K, De Baere I, Van Paepegem W, et al. Direct fracture toughness determination of a ductile epoxy poly mer from digital image correlation measurements on a single edge notched bending sample. *Polym Test* 2015; 42: 199 207.
37. Chawla KK. *Ceramic matrix composites*. London: Chapman & Hall, 1993.